0022-3565/11/3363-661–671
THE JOURNAL OF PHARMACOLOGY AND EXPERIMENTAL THERAPEUTICS
U.S. Government work not protected by U.S. copyright
JPET 336:661–671, 2011

Vol. 336, No. 3
175679/3669560
Printed in U.S.A.

Effect of Phospholipidosis on the Cellular Pharmacokinetics of Chloroquine[S]

Nan Zheng, Xinyuan Zhang, and Gus R. Rosania

Department of Pharmaceutical Sciences, College of Pharmacy, University of Michigan, Ann Arbor, Michigan (N.Z., G.R.R.); and Office of Generic Drugs, Center for Drug Evaluation and Research, United States Food and Drug Administration, Rockville, Maryland (X.Z.)

Received September 28, 2010; accepted December 13, 2010

ABSTRACT

In vivo, the weakly basic, lipophilic drug chloroquine (CQ) accumulates in the kidney to concentrations more than a thousand-fold greater than those in plasma. To study the cellular pharmacokinetics of chloroquine in cells derived from the distal tubule, Madin-Darby canine kidney cells were incubated with CQ under various conditions. CQ progressively accumulated without exhibiting steady-state behavior. Experiments failed to yield evidence that known active transport mechanisms mediated CQ uptake at the plasma membrane. CQ induced a phospholipidosis-like phenotype, characterized by the appearance of numerous multivesicular and multilamellar bodies (MLBs/MVBs) within the lumen of expanded cytoplasmic vesicles. Other induced phenotypic changes including changes in the volume and pH of acidic organelles were measured, and the integrated effects of all these changes were computationally modeled to establish their impact on intracellular CQ mass accumulation. Based on the passive transport behavior of CQ, the measured phenotypic changes fully accounted for the continuous, nonsteady-state CQ accumulation kinetics. Consistent with the simulation results, Raman confocal microscopy of live cells confirmed that CQ became highly concentrated within induced, expanded cytoplasmic vesicles that contained multiple MLBs/MVBs. Progressive CQ accumulation was increased by sucrose, a compound that stimulated the phospholipidosis-like phenotype, and was decreased by bafilomycin A1, a compound that inhibited this phenotype. Thus, phospholipidosis-associated changes in organelle structure and intracellular membrane content can exert a major influence on the local bioaccumulation and biodistribution of drugs.

Introduction

Xenobiotics can accumulate and reach very high concentrations in specific sites in the body because of active transport across cellular membranes, binding and partitioning into cellular components, or sequestration within organelles driven by pH gradients and transmembrane electrical potentials present across phospholipid bilayers. For example, more than 30 years ago, de Duve et al. (1974) discovered that weakly basic molecules would accumulate within lysosomes by an ion-trapping mechanism. Ion trapping arises when a phospholipid bilayer separates two compartments of different pH levels. Under these conditions, basic membrane-permeant lipophilic molecules become protonated and charged preferentially in the acidic compartment. Because of the lowered membrane permeability of the charged form of the molecule, the molecule becomes concentrated in the acidic compartment. Since then, many weakly basic, lipophilic small molecules have been reported to be sequestered within lysosomes or other acidic, membrane-bound intracellular compartments through passive ion trapping (Gong et al., 2007; Hayeshi et al., 2008; Bawolak et al., 2010).

However, detailed mass measurements have revealed that de Duve's classic ion trapping mechanism often underestimates the extent of sequestration of many weakly basic compounds within acidic endolysosomal organelles (Duvvuri and Krise, 2005; Zhang et al., 2010). In fact, intracellular accu-

This work was supported by the National Institutes of Health National Institute of General Medical Sciences [Grant R01-GM078200] (to G.R.R.).

The views presented in this article are those of the author (X.Z.) and do not necessarily reflect those of the Food and Drug Administration.

Article, publication date, and citation information can be found at http://jpet.aspetjournals.org.

doi:10.1124/jpet.110.175679.

[S] The online version of this article (available at http://jpet.aspetjournals.org) contains supplemental material.

ABBREVIATIONS: MLB, multilamellar body; MVB, multivesicular body; CQ, chloroquine; MDCK, Madin-Darby canine kidney cells; DMEM, Dulbecco's modified Eagle's medium; Cim, cimetidine; Gua, guanidine; TEA, tetraethylammonium; DPBS, Dulbecco's phosphate-buffered saline; Baf, bafilomycin A1; HC3, hemicholinium-3; HCor, hydrocortisone; 3MA, 3-methyladenine; FITC, fluorescein isothiocyanate; FD, FITC-dextran; BCECF-AM, 2′,7′-bis-(2-carboxyethyl)-5-(and-6)-carboxyfluorescein, acetoxymethyl ester; LTG, LysoTracker Green; Suc, sucrose; OCT, organic cation transporter; FCCP, carbonyl cyanide *p*-trifluoromethoxyphenylhydrazone; EM, electron microscopy; PMAT, plasma membrane monoamine transporter; TEM, transmission electron microscopy.

mulation of weak bases may also be influenced by active transport mechanisms or by the many concomitant changes in endolysosomal organelle structure and function, including alterations in pH and changes in membrane traffic, leading to the formation of new endolysosomal organelles with unique characteristics (Heuser, 1989; Honegger et al., 1993). In some cell types, exposure to lipophilic weak bases induces a peculiar phenotype, "phospholipidosis" (Reasor and Kacew, 2001), characterized by the formation of numerous, phospholipid- and cholesterol-rich multivesicular bodies (MLBs) and multilamellar bodies (MVBs). Physiologically, MLBs/MVBs are late endosomal compartments that normally form as a result of the activation of the ubiquitin-dependent membrane protein sorting and degradation pathway (Gruenberg and Stenmark, 2004; Piper and Katzmann, 2007; Saftig and Klumperman, 2009).

Previously, we developed a computational model of cell pharmacokinetics to predict the intracellular accumulation and transcellular transport properties of small molecules across the cell monolayer (Zhang et al., 2006, 2010). By using the weakly dibasic, high-solubility drug chloroquine (CQ) (pK_{a_1} = 9.96 and pK_{a_2} = 7.47) as a test compound, the model was capable of capturing the transcellular transport kinetics for the first 4 h of drug treatment but underestimated the intracellular accumulation beyond the first 5 min of incubation (Zhang et al., 2010). Experimentally, the initial rates of transport of CQ across cell monolayers were directly proportional to CQ concentrations in donor compartment. In addition, the transport of CQ across Madin-Darby canine kidney (MDCK) monolayers in the presence of a transcellular concentration gradient was similar in both apical-to-basolateral and basolateral-to-apical directions. No saturation or nonlinear kinetics were observed at CQ concentrations <500 μM, as expected from a passive transport mechanism (Zhang et al., 2010).

Here, we present an alternative hypothesis to explain CQ accumulation: that drug-induced phospholipidosis corresponds to an inducible, weak base disposition system, a mechanism promoting CQ sequestration within cells. We performed a detailed quantitative analysis of CQ pharmacokinetics in MDCK cells, a cell line that stably expresses the differentiated properties of distal tubular epithelial cells (Rindler et al., 1979), extensively accumulates CQ, and exhibits a marked phospholipidosis-like response (Hostetler and Richman, 1982) corresponding to the phospholipidosis phenotype reported in the kidney cells of CQ-treated patients (Müller-Höcker et al., 2003). The potential involvement of active transporters and plasma membrane-mediated uptake mechanisms was evaluated in the presence of extracellular pH changes, sodium-free medium, and organic cation transporter inhibitors.

Although the CQ concentration in plasma ranges between 10 and 250 nM (Walker et al., 1983; Bergqvist et al., 1985), cells lining the distal tubules are exposed to 10 to 300 μM CQ, corresponding to the concentrations measured in the urine of human subjects (Bergqvist et al., 1985). Therefore, clinically relevant urine concentrations (0–200 μM) of CQ were used to mimic the physiological conditions of the distal tubule and used as input parameters to mathematically model transport behavior of CQ. Simulation results were compared with experimental measurements of intracellular CQ mass in dose-response and time course experiments, under conditions that either enhanced the phospholipidosis effect [cotreatment with sucrose (Wilson et al., 1987; Helip-Wooley and Thoene, 2004)] or inhibited vacuolation [cotreatment with bafilomycin A1 (Morissette et al., 2009)].

Materials and Methods

Cell Culture. MDCK cells were purchased from American Type Culture Collection (Manassas, VA) and grown in Dulbecco's modified Eagle's medium (DMEM) (GIBCO; Invitrogen, Carlsbad, CA) containing 10% fetal bovine serum (GIBCO; Invitrogen), 1× nonessential amino acids (GIBCO; Invitrogen), and 1% penicillin/streptomycin (GIBCO; Invitrogen) at 37°C in a humidified atmosphere with 5% CO_2. MDCK cells were seeded at a density between 1 and 2 × 10^5 cells/cm^2 and were grown until a cell monolayer was formed as suggested by visual inspection.

Drugs and Chemicals. Chloroquine diphosphate, cimetidine (Cim), guanidine (Gua), and tetraethylammonium (TEA) were obtained from Sigma-Aldrich (St. Louis, MO) and dissolved in Dulbecco's phosphate-buffer saline (DPBS) (GIBCO; Invitrogen) at a concentration of 100 mM for storage at 4°C. Bafilomycin A1 (Baf), hemicholinium-3 (HC3), and hydrocortisone (HCor) (Sigma-Aldrich) were dissolved in dimethyl sulfoxide (Sigma-Aldrich) to a final concentration of 5 μM (Baf) or 50 mM (HC3 and HCor) for storage at −20°C. 3-Methyladenine (3MA) (Sigma-Aldrich) was dissolved in warm DMEM at a concentration of 10 mg/ml immediately before use. Fluorescein isothiocyanate (FITC)-dextran (FD) (Sigma-Aldrich) was dissolved in DPBS at a concentration of 10 mg/ml for storage at 4°C. Fluorescent dyes including BCECF-AM, LysoTracker Green (LTG), and Hoechst 33342 (Molecular Probes; Invitrogen) were stored according to the manufacturer's instructions.

Measurement of LTG Fluorescence Intensity, Distribution, and LTG-Labeled Organelle Volumes. MDCK cells were grown on an optical bottom plate or chamber glass, subjected to various CQ treatments, stained with 0.5 μM LTG for 30 min, and subjected to microscopic analysis in situ. A Nikon TE2000S epifluorescence microscope with standard mercury bulb illumination, coupled to a charge-coupled device camera (Roper Scientific, Tucson, AZ), with a 20× objective ((Nikon Plan Fluor ELWD 20×) or a 100× oil immersion objective (Nikon CFI Plan Fluor 100×H oil), and a triple-pass DAPI/FITC/TRITC filter set (Chroma Technology Corp., Brattleboro, VT) was used to image the LTG-labeled cells. The 12-bit grayscale images were acquired with the FITC channel and background-subtracted. The LTG-labeled expanded vesicles (or the MLBs/MVBs contained within) were manually outlined with the Circular Region tool in MetaMorph software (Molecular Devices, Sunnyvale, CA). The volume and surface area of individual vesicles were calculated assuming a spherical shape. Fluorescence volume density was calculated as integrated intensity divided by vesicle volume. The total vesicular volume/surface area per cell under each treatment at each time point (0, 1, 2, or 4 h) was determined using 10 cells (Supplemental Fig. 1, validation of method). Contrast and brightness were adjusted to the same level in all figures.

Raman Confocal Microscopy of CQ Distribution. MDCK cells were seeded on cover glass until confluent. CQ-treated cells were exposed to 10 μM CQ for 12 h, followed by 100 μM CQ for 2 h, and briefly washed in DPBS buffer before mounting on microscope slides. The induced Raman spectrum of solid CQ salt, 100 mM CQ solution in DPBS, and vesicular/cytosolic regions of the cells under various treatment conditions was acquired with a Renishaw inVia confocal Raman microscope coupled with a Nikon CFI Plan Fluor 100×H oil immersion objective and a charge-coupled device detector. The excitation wavelength was 514 nm. The exposure time was 30 s for each measurement, with spectral resolution set to 1.5 cm^{-1}, scanning from 400 to 3200 cm^{-1}. All spectra were smoothened, baseline-subtracted, and normalized to the highest peak with an ACD/UV-IR Processor (ACD/Labs, Toronto, ON, Canada). To deter-

mine the effect of pH on the Raman spectra of CQ, spectra of 100 mM CQ solution in pH 7, 6, and 5 buffers were also acquired.

Measurement of Lysosomal, Cytosolic, and Extracellular pH. pH measurements were performed using published methods (Nilsson et al., 2003). To measure lysosomal pH, MDCK cells were incubated with 0.2 mg/ml FD in DMEM for 24 h in the dark before drug treatments. FD-loaded cells were washed twice with warm DPBS buffer and incubated in CQ-DMEM with or without sucrose (Suc) or Baf for 1, 2, 3, or 4 h. To measure cytosolic pH, BCECF-AM was added to a final concentration of 2 mg/ml during the last 30 min of drug treatment in the dark. At the end of treatments, cells on plate were washed twice with cold buffer before ratiometric analysis of the pH-sensitive FD or BCECF-AM fluorescence signal. Fluorescence data were acquired with a BioTek Synergy 2 Microplate Reader using an Ex485/20-Em528/20 filter set and an Ex450/50-Em528/20 filter set. Background fluorescence was acquired with dye-free untreated cells. Standard curves were obtained by first preloading untreated cells with 0.2 mg/ml FD for 24 h or 2 mg/ml BCECF-AM for 30 min, then equilibrating with 10 μg/ml nigericin in different pH buffer, and finally scanning with the same filter sets as mentioned above. The fluorescence ratio (FR) was calculated as

$$\mathrm{FR} = \frac{\mathrm{F485}_i - \mathrm{F485}_{\mathrm{bg}}}{\mathrm{F450}_i - \mathrm{F450}_{\mathrm{bg}}}$$

where $\mathrm{F485}_i$ and $\mathrm{F450}_i$ stand for integrated fluorescent intensity from the ith well of cells under excitation 485 and 450 nm, respectively, and the subscript bg indicates background fluorescence. Fluorescence ratio values were plotted against known pH values to create a standard curve or compared with the standard curve to calculate pH. Extracellular pH was measured with a Corning pH meter 430 at designated time points. The average vesicular pH, cytosolic pH, and extracellular pH were reported as the mean ± S.D. over a 4-h incubation period with each time point measured from three independent experiments.

Measurement of Cell Volume. Cells were detached from the tissue culture plates after drug treatment by incubating them with 0.25% trypsin-EDTA (GIBCO; Invitrogen) for 15 min. The rounded, detached cells were imaged with a Nikon TE2000S inverted microscope under brightfield illumination with a 20× objective (Nikon CFI Plan Fluor 20×). In the images, the perimeters of the cells were manually outlined with the Circular Region Tool in MetaMorph, and cell volume was calculated from the radius of the outlined perimeter, assuming a spherical shape. For each treatment, 10 brightfield images (more than 100 cells) were collected after 1, 2, 3, or 4 h. The average cell volume was reported as the mean ± S.D. over 4 h of treatment.

Measurement of the Cellular Partition Coefficient of CQ. MDCK cells were grown on tissue culture dishes treated with 50 μM CQ for 4 h to induce vacuolar expansion and MLBs/MVBs. After this induction period, the cells were permeabilized with 0.1% saponin in DPBS buffer for 30 min to extract soluble cellular components while leaving lipids, DNA, and associated, insoluble cytoskeletal components. Permeabilized cells were then incubated with 100 μM CQ for 1 h, washed twice, and centrifuged. Cellular lipids and associated molecules were extracted from the pellet with 1% Triton X-100 in DPBS for 1 h. Nuclei and other insoluble debris were spun down, and the amount of extracted CQ in the supernatants was determined by measuring absorbance at 343 nm using Microplate Reader. On the basis of electron micrographs, we estimated a Triton X-100-extractable, 5% lipid volume fraction in the cell. CQ concentration partitioned into the cellular lipid structures was calculated as bound CQ amount divided by the estimated lipid volume for the cells. The lipid partition coefficient was calculated as the logarithm of the lipid/buffer CQ concentration ratio.

Probing the Mechanism of CQ Uptake with Transport Inhibitors. To study the effect of active cation transporters on CQ uptake, MDCK cells on 24-well tissue culture plates (Costar or Nunc) were incubated with 50 μM CQ in 0.5 ml of bicarbonate-free transport buffer (140 mM sodium chloride, 5.4 mM potassium chloride, 1.8 mM calcium chloride, 0.8 mM magnesium chloride, 25 mM *d*-glucose, and 10 mM HEPES, pH 5.5, 6.5, 7.4, and 8.5) or sodium-free, choline-based transport buffer (substitute sodium chloride with choline chloride in the above transport buffer) at 37°C. To study the effect of autophagy, energy supply, vacuolar ATPase, organic cation transporters (OCTs) and pre-expanded lysosomal volume on CQ uptake, MDCK cells were incubated in 0.5 ml of DMEM containing 50 μM CQ in the presence or the absence of 10 mg/ml 3MA (autophagy inhibitor), 5 μM FCCP (mitochondrial uncoupling agent that disrupts ATP synthesis and cellular metabolism), 10 nM Baf (vacuolar H^+/ATPase inhibitor that disrupts endolysosomal pH gradients), 500 μM Cim (OCT inhibitor), 500 μM Gua (OCT inhibitor), 500 μM HC3 (OCT inhibitor), 500 μM TEA (OCT substrate/inhibitor), 20 μM HCor (a hormone that stimulates OCT expression), or 0.1 M Suc (a treatment that enhances the phospholipidosis phenotype without competing with CQ uptake). Cells cotreated with CQ and Suc or HCor were preincubated with 0.1 M sucrose or 20 μM hydrocortisone in DMEM for 24 or 48 h, respectively, before the experiments. CQ uptake was measured 0.5, 5, 15, 30, 60, 120, 180, or 240 min after the beginning of the incubation with Suc or Baf or 30 and 240 min after the beginning of incubation with other compounds. For CQ uptake measurements, three of the four replicates under the same treatment were briefly washed with cold buffer and lysed in 1% Triton X-100 for 1 h. The lysates were centrifuged at 15,000 rpm for 10 min, and the supernatant was collected for CQ measurement by reading absorbance at 343 nm using Microplate Reader. Intracellular CQ mass was normalized by the number of cells per well as evaluated by counting cells in the fourth replicate well. Background signal from 0 μM CQ treatment was subtracted, and CQ mass was calculated with the aid of a standard curve. The results are expressed as mean ± S.E.M. from three independent experiments for each time point.

Measurement of MLB/MVB Morphology. For transmission electron microscopy, MDCK cells were grown on a tissue culture dish (Falcon; BD Biosciences Discovery Labware, Bedford, MA), incubated with 50 μM CQ for 4 h, washed twice with serum-free DMEM, fixed with 2.5% glutaraldehyde in 0.1 M Sorensen's buffer at pH 7.4 at 37°C, and washed three times for 5 min each with 0.1 M Sorensen's buffer. Cells were fixed with 1% osmium tetroxide in 0.1 Sorensen's buffer for 15 min at room temperature and washed three times with double-distilled water. Cells were incubated with 8% uranyl acetate in double-distilled water for 1 h at room temperature, dehydrated in a graded ethanol-water series (50, 70, 90, and 100%, 5 min each), infiltrated in Epon resin, and polymerized at 60°C overnight. Cells were sectioned and photographed with a Phillips CM-100 transmission electron microscope at magnifications from 2600 to 96,000×. More than five cells were photographed for control and treated cells under each condition. Quantitative morphological analysis of EM images was performed with MetaMorph.

Mathematical Modeling of CQ Uptake. A multicompartment, constant-field, fixed-parameter mathematical model (Trapp and Horobin, 2005) was adapted to predict the passive membrane potential and pH-dependent ion-trapping behavior of CQ in MDCK cells. The original model was modified to incorporate the gradual volume expansion of the endolysosomal compartment induced by CQ, coupled to changes in extracellular concentration accompanying pronounced, intracellular CQ sequestration. In brief, the total change in CQ mass with time in each compartment was expressed by eqs. 1 to 4:

$$\frac{d\mathrm{M_e}}{dt} = -A_\mathrm{c} \times J_\mathrm{e,c} \tag{1}$$

$$\frac{d\mathrm{M_c}}{dt} = A_\mathrm{c} \times J_\mathrm{e,c} - A_\mathrm{m} \times J_\mathrm{c,m} - A_\mathrm{l} \times J_\mathrm{c,l} \tag{2}$$

$$\frac{d\mathrm{M_m}}{dt} = A_\mathrm{m} \times J_\mathrm{c,m} \tag{3}$$

$$\frac{dM_l}{dt} = A_l \times J_{c,l} \quad (4)$$

where M stands for the total mass, J indicates the flux, A and V indicate the membrane surface area and volume, respectively, of the specific subcellular compartments as indicated by the subscripts e, c, m, and l [extracellular compartment, cytosol, mitochondria, and (acidic) lysosomes compartment, respectively], and A_c indicates the plasma membrane area of the cell. The comma between two subscripts means "to" (e.g., "$J_{c,m}$" represents the flux from cytosol to mitochondria). With extracellular volume, cell volume, and mitochondria volume constant and lysosomal volume change, the concentration change in each compartment was expressed by eqs. 5 to 8:

$$\frac{dC_e}{dt} = -\frac{A_c}{V_c} \times J_{e,c} \quad (5)$$

$$\frac{dC_c}{dt} = \frac{A_c}{V_c} \times J_{e,c} - \frac{A_m}{V_c} \times J_{c,m} - \frac{A_l}{V_c} \times J_{c,l} \quad (6)$$

$$\frac{dC_m}{dt} = \frac{A_m}{V_m} \times J_{c,m} \quad (7)$$

$$\frac{dC_l}{dt} = \frac{A_l}{V_l} \times J_{c,l} - \frac{dV_l}{dt} \times \frac{C_l}{V_l} \quad (8)$$

For CQ, the total flux is contributed by a neutral form and two ionized forms with one or two positive charges (Zhang et al., 2010). The total flux across membrane as contributed by three species can be calculated with Fick's equation and the Nernst-Planck equation:

$$J_{o,i} = \boldsymbol{P}_n(\boldsymbol{f}_{n,o}C_o - \boldsymbol{f}_{n,i}C_i) + \boldsymbol{P}_{d1}\frac{N_{d1}}{e^{N_{d1}}-1}(\boldsymbol{f}_{d1,o}C_o - \boldsymbol{f}_{d1,i}C_i e^{N_{d1}}) + \boldsymbol{P}_{d2}\frac{N_{d2}}{e^{N_{d2}}-1}(\boldsymbol{f}_{d2,o}C_o - \boldsymbol{f}_{d2,i}C_i e^{N_{d2}}) \quad (9)$$

where subscripts o and i indicate the outer and inner compartment, and n, d1, and d2 indicate neutral form, ionized form with one charge, and ionized form with two charges, respectively. $\boldsymbol{P}$ is the permeability across the bilayer membranes, and it was estimated on the basis of the logarithm of the octanol/water partition coefficient of CQ ($\log P_{o/w}$) calculated with ChemAxon MarvinSketch 5.1.4 (http://www.chemaxon.com) (Trapp and Horobin, 2005). $\boldsymbol{f}$ represents the ratio of the activities (a_n, a_{d1}, and a_{d2}) and the total concentration. It can be calculated from lipid fraction and ionic strength in each compartment and the sorption coefficient for each species as estimated from $\log P_{o/w}$ (Trapp and Horobin, 2005; Zhang et al., 2006) or the measured cellular partition coefficient (Zhang et al., 2010). In eq. 9, $N = zEF/(RT)$, where $z = +1$ for N_{d1} (ionized base with one charge) and $z = +2$ for N_{d2} (ionized base with two charges) and E, F, R, and T are membrane potential, Faraday constant, universal gas constant, and absolute temperature, respectively. The rate of change in the vesicular volume was derived by fitting the volume measurement at each time point with a linear model. When CQ binding to MLBs/MVBs was simulated, the measured cellular partition coefficient of CQ was used to estimate $\boldsymbol{f}$. The ordinary differential equations were numerically solved with MATLAB ODE15s solver using the average value of each parameter to plot a kinetic curve of CQ intracellular accumulation. A model validation/consistency check was performed by summing CQ mass in all compartments during the simulation, confirming that total CQ mass in the system stays constant (mass balance).

Parameter Sensitivity and Error Propagation Analysis. To determine whether variations in individual parameters would lead to a large variation in prediction, sensitivity analysis was performed by systemically changing one parameter at a time and plotting predictions against parameter values. In addition, Monte Carlo simulations were performed to assess the distribution of CQ accumulation values that would be consistent with uncertainties or experimental error of the input parameters. Parameter ranges were obtained on the basis of the error of experimental measurements or variations in the published literature reports (Supplemental Table S1). MATLAB ODE15s solver was used to run 10,000 simulations during which simulation parameters were randomly sampled from uniform distributions within the range of parameter values (Supplemental Table S1). Histograms of simulation results were plotted with R (http://www.r-project.org).

Results

CQ-Treated MDCK Cells Undergo Marked Changes in Organelle Structure and Membrane Organization. Electron microscopy was performed to study the effects of CQ on the membrane and organelle structure of MDCK cells during the course of a 4-h incubation period. Most strikingly, CQ induced the formation of numerous MLBs/MVBs within the lumen of expanded cytoplasmic vesicles (Fig. 1). The expanded vesicles were approximately 1.50 ± 0.34 μm (n = 20) in diameter. Within these expanded vesicles, there were many MLBs of 0.42 ± 0.025 μm (n = 10) in diameter and MVBs of 0.39 ± 0.03 μm (n = 10) in diameter. For MLBs, the spacing between membrane layers ranged from 24.0 to 29.2 nm (25.7 ± 2.2 nm), and the apparent thickness of each layer varied from 22.5 to 24.0 nm (23.2 ± 0.7 nm). For MVBs, the internal vesicles varied in size between 50 and 100 nm in diameter. It was generally the case that in the presence of CQ, each expanded vesicle contained several MLBs/MVBs. Without CQ treatment, control cells completely lacked these features (data not shown).

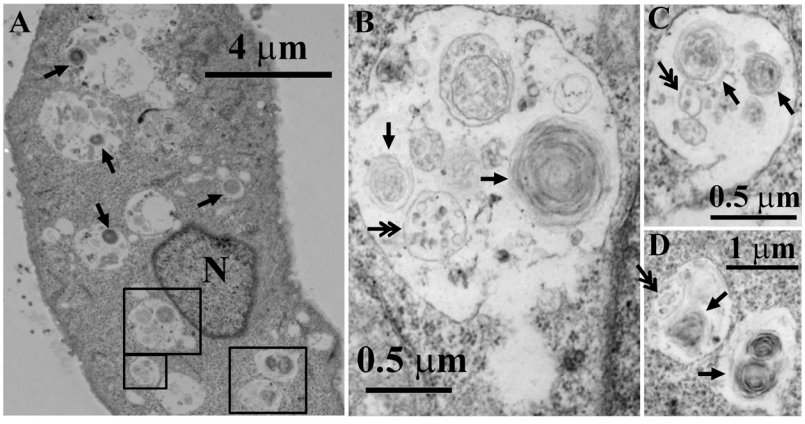

Fig. 1. CQ induces a phospholipidosis-like phenotype characterized by the formation of many MLBs/MVBs in MDCK cells. MDCK cells were treated with 50 μM CQ for 4 h followed by transmission electron microscopy analysis. A–D, MDCK cells with enlarged vesicular compartments or MLBs/MVBs comprised of intraluminal MLBs (single arrows) or MVBs (double arrows). N, nucleus. Original magnification, 7900× (A), 34,000× (B and C), and 13,600× (D).

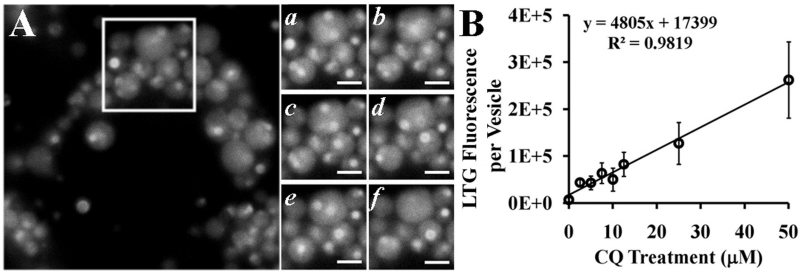

Fig. 2. CQ-induced nonuniform distribution (A) and dose-dependent accumulation (B) of LTG within the LTG-positive vesicles in MDCK cells. A, at the end of a 4-h incubation with 50 μM CQ, LTG fluorescence within individual vesicles was concentrated within small particles of 0.3 to 0.4 μm in diameter, which underwent Brownian motion within the confines of the enlarged vesicles. These particles corresponded in shape and size to MLBs/MVBs observed by electron microscopy (Fig. 1). Images a to f were taken at 4-s intervals to show the Brownian movement of the bright MLBs/MVB particles within the lumen of the expanded vesicles. Scale bar, 2 μm. B, after a 4-h incubation with different amounts of CQ, the fluorescence volume intensity per vesicle increased with CQ treatment. Five cells (more than 300 vesicles) were measured under the same treatment.

Induced MLBs/MVBs Sequester Weakly Basic Lipophilic Molecules. LTG is a weakly basic fluorescent probe that labels acidic organelles within cells by the ion-trapping mechanism. Fluorescence micrographs of CQ-treated cells incubated with LTG showed LTG fluorescence accumulation in enlarged vesicles ranging from 1 to 2 μm in diameter. Most remarkable, at high magnification, LTG distribution within each one of the expanded vesicles was clearly associated with intraluminal MLBs/MVBs (Fig. 2A). In many of these vesicles, LTG was clearly localized to multiple internal vesicles of approximately 0.34 ± 0.06 μm (n = 20) in diameter, consistent with the numbers and diameters of the MLBs/MVBs previously observed by electron microscopy. Based on quantitative image analysis, we calculated that accumulation of LTG fluorescence bound to the MLBs/MVBs was at least 4.7 ± 0.5 (n = 20)-fold greater than its accumulation in the lumen of the expanded vesicle. LTG-labeled MLBs/MVBs appeared to move by Brownian motion, within the confines of the outer membrane bounding the expanded vesicles (Fig. 2A, a–f; Supplemental Movie 1). Increasing CQ concentrations did not inhibit LTG fluorescence accumulation. Instead, the accumulation of LTG fluorescence in the vacuoles was directly dependent on the concentration of CQ used for treatment, showing no evidence of competition or saturation (Fig. 2B).

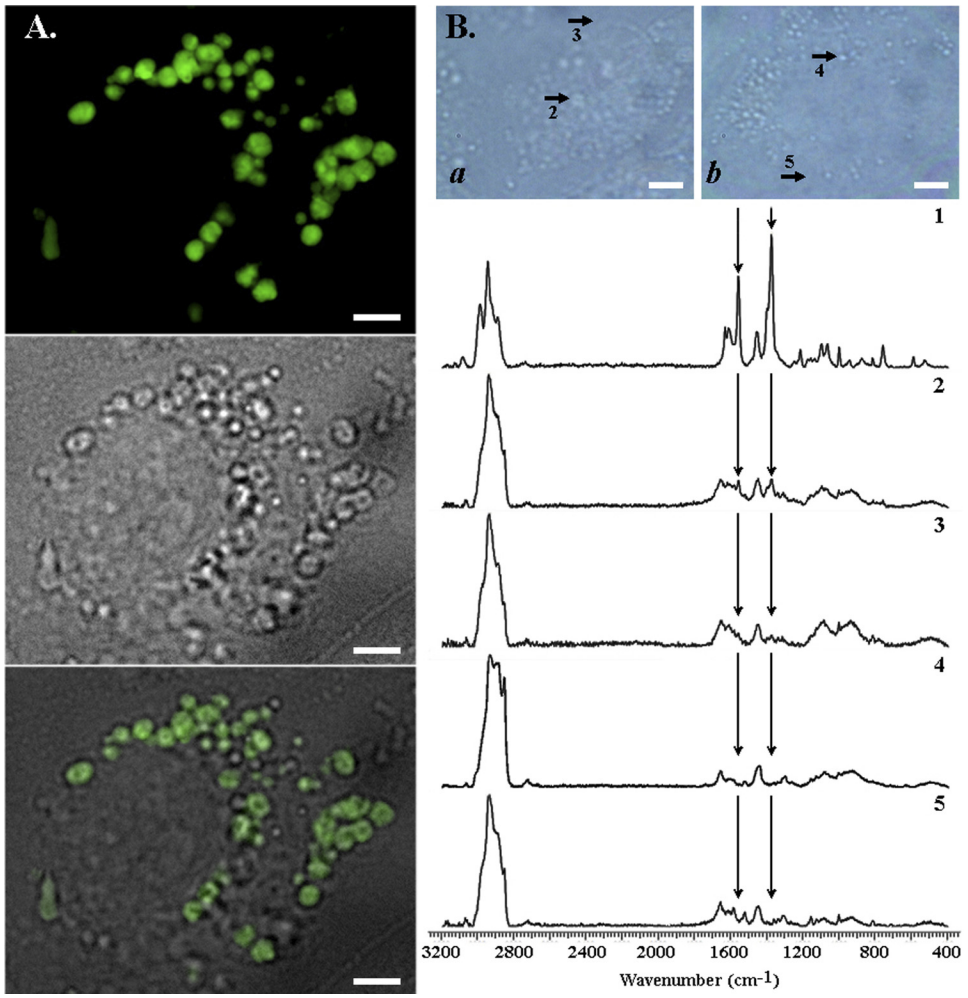

Fig. 3. CQ accumulates within enlarged MLB/MVB-positive vesicles. MDCK cells were treated with 10 μM CQ for 12 h, which primes them for vacuolar expansion and MLB/MVB formation, followed by 100 μM CQ for 2 h before imaging. For fluorescence microscopy, cells were incubated with 0.5 μM LTG for 30 min immediately before imaging. A, LTG fluorescence (top) and the corresponding brightfield image (middle) of a representative CQ-treated cell was merged (bottom), showing the highly heterogeneous LTG fluorescence associated with MLB/MVBs within the expanded cytoplasmic vesicles. Scale bar, 4 μm. B, analysis of intracellular CQ distribution by confocal Raman microscopy. Top, brightfield image showing 100 μM CQ-treated (a) and untreated (b) cells from which spectra were acquired. Scale bar, 5 μm. Bottom, spectrum 1 was acquired from 100 mM CQ solution in buffer, as reference. Spectra 2 and 3 were acquired from the vesicles and cytosol of treated cells, respectively; spectra 4 and 5 were acquired from the vesicles and cytosol of untreated cells. In these spectra, CQ-specific Raman vibrational peaks (around wavenumbers 1370 and 1560) were identified on the basis of spectrum 1. The CQ-specific Raman signal was mostly localized within the expanded vesicles of CQ-treated cells.

CQ Accumulates within Induced, Expanded Vesicles. The MLBs/MVB-containing, LTG-labeled vesicles induced by CQ corresponded to large, clear vacuoles apparent by brightfield transmitted light microscopy (Fig. 3A). Confocal Raman microscopic imaging was performed in CQ-treated (Fig. 3B, a) and untreated (Fig. 3B, b) cells. The signature Raman signal of CQ (Fig. 3B, spectrum 1, arrows, 1370 and 1560 cm^{-1}) was present in the vacuoles observed by brightfield transmitted light microscopy (Fig. 3B, spectrum 2), yet the CQ signal was mostly undetectable in the vesicle-free regions of the same cells (Fig. 3B, spectrum 3). In control experiments, the signal intensity of the Raman vibrational peaks of CQ at 1370 and 1560 cm^{-1} were constant between pH 7 and 5 (data not shown), so differences in the pH of intracellular compartments cannot explain the observed, spectral differences in Raman signal. Furthermore, a CQ signal was completely absent from untreated cells (Fig. 3B, spectra 4 and 5). Given their small volume, the presence of Raman signals within the vacuoles of CQ-treated cells confirmed that CQ is highly concentrated within these vesicles.

CQ Uptake Is Coupled to Induction of Phospholipidosis-Like Phenotype and Cannot Be Inhibited by OCT Inhibitors. Consistent with the neutral, membrane-permeant form of CQ being mostly responsible for its passive cellular uptake, CQ uptake within the first 30 min was significantly reduced by lowering of extracellular pH (Fig. 4A) but was not significantly affected by the presence of OCT inhibitors and a stimulator (Cim, Gua, HC3, TEA, or HCor) nor by the substitution of sodium with chloride in the transport buffer (Fig. 4B). Incubation at 4°C reduced CQ uptake in the first 30 min, consistent with inhibited passive diffusion at low temperature, whereas preincubation with 0.1 M sucrose-DMEM, a treatment that induced lysosomal volume expansion, stimulated CQ uptake by 32% during this time (Fig. 4B). Bafilomycin A1, a vesicular ATPase inhibitor that hampers the acidification of lysosomes, reduced CQ uptake by 21% within the first 30 min of CQ incubation, whereas the autophagy inhibitor 3MA did not (Fig. 4B). After a 4-h treatment, a close correlation between CQ uptake (Fig. 4C) and lysosomal volume expansion (Fig. 4D) was observed: in cells treated with Baf and FCCP, CQ-induced vesicular expansion

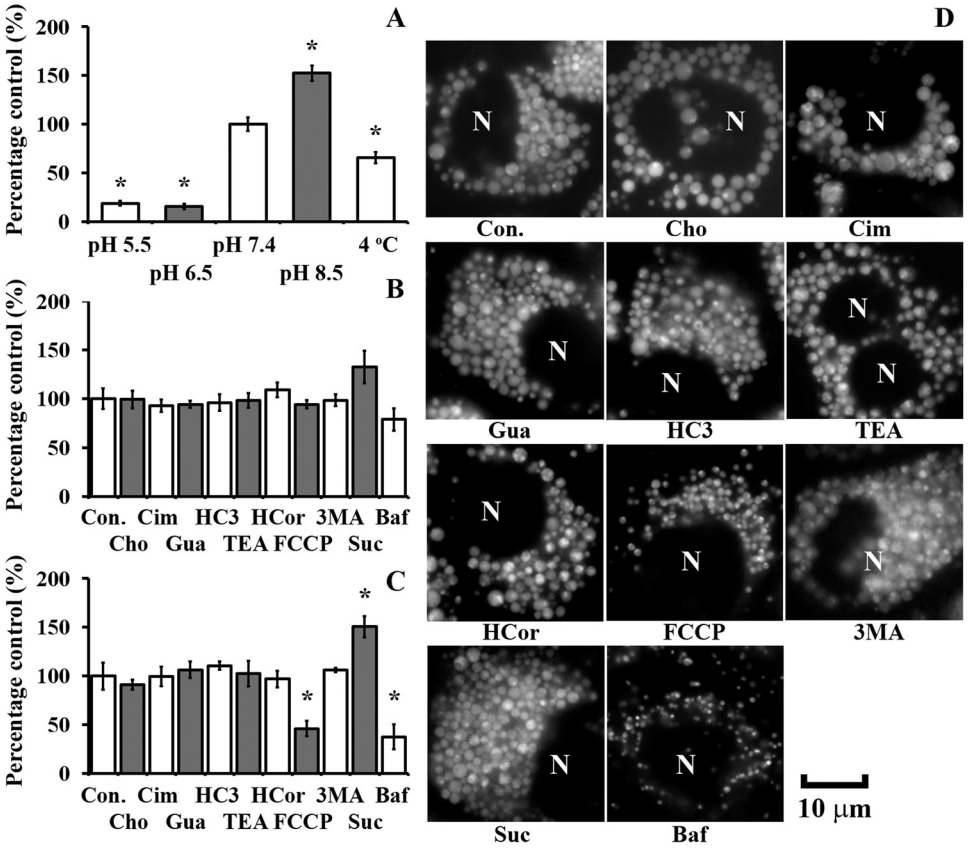

Fig. 4. Temperature- and pH-dependent CQ uptake parallels the induced phospholipidosis effect and is insensitive to pharmacological inhibitors of organic cation transport. A, within 30 min CQ uptake (50 μM) into MDCK cells was significantly reduced by lowering extracellular pH and lowering the temperature. Uptake experiments were performed in transport buffer. Control experiments were performed at pH 7.4 and 37°C. B, within 30 min of incubation, CQ uptake (50 μM) and cellular vacuolation were not significantly perturbed by inhibitors of autophagy or active transport. Preincubation with 0.1 M sucrose in DMEM increased CQ uptake within 30 min, whereas cotreatment with bafilomycin A1 inhibited CQ uptake, but the difference was not significant. Uptake experiments were performed in choline-based transport buffer (Cho) and DMEM (all the other conditions). C and D, at the end of a 4-h incubation, CQ uptake and LTG-positive vesicular expansion were partially inhibited by FCCP, significantly suppressed by bafilomycin A1, but not reduced by the OCT inhibitor/stimulator, the autophagy inhibitor 3MA, or the sodium-free extracellular buffer. Con., control, 50 μM CQ only; Cho, 50 μM CQ in choline-based transport buffer; Cim, 500 μM cimetidine; HC3, 500 μM hemicholinium-3; Gua, 500 μM guanidine; TEA, 500 μM tetraethylammonium; HCor, 20 μM hydrocortisone; FCCP, 5 μM FCCP; 3MA, 10 mg/ml 3-methyladenine; Suc, 0.1 M sucrose; Baf, 10 nM bafilomycin A1. Data are presented as the mean ± S.E.M from three experiments. *, significant difference from control using an unpaired Student's t test ($p < 0.05$). N, nucleus. Scale bar, 10 μm.

was significantly suppressed and so was the cellular uptake; in cells treated with transporter inhibitors, sucrose or 3MA, no significant reduction in vesicular expansion nor cellular uptake was observed compared with that for CQ treatment alone. In the presence of Suc, 3MA, or other OCT inhibitors, we also observed LTG fluorescence accumulated in association with the MLBs/MVBs present within the induced, expanded vacuoles, as was observed in cells treated with CQ alone.

CQ Affected Organelle Volume and pH. LTG-positive (acidic) organelle volume and pH, as well as cell volume and cytosolic pH, were measured at various time points, during a 4-h CQ incubation period (Table 1). Experiments were also performed in the presence of 0.1 M Suc, a treatment that perturbs endolysosomal membrane traffic and promotes a phospholipidosis-like phenotype (Helip-Wooley and Thoene, 2004). CQ uptake measurements were also performed in the presence of 10 nM Baf, a treatment that inhibits the phospholipidosis effect. CQ-induced vacuolation was greater in the presence of sucrose compared with that in cells treated with CQ alone and was inhibited by Baf (Table 1). Total cell volume significantly expanded in Suc but not in CQ or CQ/Baf (Table 1). CQ (with or without Suc or Baf) increased vesicular pH during a 4-h incubation period, but cytosolic pH was not significantly perturbed (Table 1). The extent of the CQ-induced vesicular pH increase was highest in the presence of Suc, intermediate with Baf, and least with CQ alone. At 200 μM CQ, toxicity became apparent, with several of the observed trends becoming reversed (Table 1). Consistent with the large buffering capacity of the extracellular medium, measurements confirmed that CQ treatments with or without Suc or Baf did not alter the extracellular pH (Table 1).

Organelle Volume and pH also Affect CQ Uptake. The effects of Suc and Baf on the pharmacokinetics of CQ were measured in dose-response and time course experiments. Upon prolonged incubation, CQ exhibited a time-dependent, gradual accumulation over a 4-h incubation period (Fig. 5). Suc treatment before CQ incubation led to the most pronounced intracellular accumulation of CQ (Fig. 5A). Baf inhibited the gradual accumulation of CQ, with cells showing a rapid uptake during the first 5 min, followed by a low, steady-state level during the next 4 h (Fig. 5A). At 50 and 100 μM, CQ accumulation over a 4-h period appeared almost linear in Suc-treated cells as well as in cells that were incubated with CQ alone (Fig. 5A).

Simulations of CQ Cellular Pharmacokinetics. Computational simulations of CQ uptake with a mathematical model that incorporates volume expansion of acidic organelles, protonated CQ binding to MLBs/MVBs, and use of the measured parameter values as input yielded CQ dose-response and time course traces that were consistent with the experimentally measured values (Fig. 5A) and well within the simulated margins of error based on physiologically relevant ranges of input parameters (Fig. 5B). The effects of Suc and Baf on CQ uptake paralleled the experimental measurements (Fig. 5A) for 25, 50, and 100 μM CQ treatments. Simulation results for 200 μM treatments tended to overpredict CQ uptake (Fig. 5A), which we ascribe to the toxic effects that were apparent at this higher dose. Overall, the accuracy of predicted cellular uptake was good for a wide range of different CQ concentrations, in the presence or absence of Suc or Baf at eight time points, with 70% of the predicted values within a factor of 2 or 86% within a factor of 3 of the measured cellular uptake values (Fig. 6). Except for the 200 μM treatment during which cellular uptake was possibly reduced by the toxic effect, most other discrepancies were observed between predictions and measurements for the first time points when the amount of cellular CQ uptake was closest to the detection limit of the instrument.

TABLE 1

Measured cellular parameters

Cellular parameters were measured during a 4-h incubation with different concentrations of CQ. pH measurements and cell volume correspond to the average over the 4-h incubation period; data correspond to the mean ± S.D. $n = 4$. Vesicle volume corresponds to the volume at the end of the 4-h treatment; data are presented as the mean ± S.D. $n = 10$.

Treatment[a]	Vesicular pH	Vesicle Volume/Cell	Vesicle Surface Area/Cell	Cytosolic pH	Cell Volume (10^3 μm^3)	Extracellular pH
		μm^3	μm^2			
Untreated	5.03 ± 0.15	21 ± 8	219 ± 74	7.4 ± 0.2	1.64 ± 0.41	7.45 ± 0.04
25 μM CQ						
CQ/Suc	**5.91 ± 0.23**[b]	**602 ± 145**	**2130 ± 349**	7.37 ± 0.02	**3.00 ± 0.14**	7.48 ± 0.03
CQ/	5.36 ± 0.28	304 ± 76	1159 ± 47	7.36 ± 0.04	1.66 ± 0.12	7.48 ± 0.03
CQ/Baf	5.55 ± 0.17	18 ± 5	189 ± 55	7.38 ± 0.03	1.74 ± 0.14	7.47 ± 0.03
50 μM CQ						
CQ/Suc	**6.08 ± 0.20**	**843 ± 176**	**2795 ± 491**	7.36 ± 0.01	**3.05 ± 0.28**	7.47 ± 0.03
CQ/	5.51 ± 0.34	**587 ± 126**	**2207 ± 1050**	7.36 ± 0.01	1.84 ± 0.05	7.47 ± 0.03
CQ/Baf	5.69 ± 0.37	19 ± 4	204 ± 24	7.35 ± 0.02	1.70 ± 0.15	7.47 ± 0.03
100 μM CQ						
CQ/Suc	**6.45 ± 0.21**	**1121 ± 343**	**2995 ± 385**	7.37 ± 0.02	**2.95 ± 0.33**	7.50 ± 0.02
CQ/	**5.81 ± 0.21**	294 ± 53	**1219 ± 234**	7.35 ± 0.04	1.83 ± 0.12	7.50 ± 0.02
CQ/Baf	**5.88 ± 0.14**	17 ± 3	178 ± 28	**7.34 ± 0.03**	1.77 ± 0.14	7.50 ± 0.02
200 μM CQ						
CQ/Suc	**6.73 ± 0.28**	**565 ± 140**	**1468 ± 351**	**7.37 ± 0.02**	**3.27 ± 0.37**	7.50 ± 0.02
CQ/	**5.98 ± 0.45**	204 ± 47	785 ± 193	**7.30 ± 0.02**	1.62 ± 0.17	7.50 ± 0.02
CQ/Baf	**6.26 ± 0.45**	17 ± 4	186 ± 32	**7.17 ± 0.04**	1.78 ± 0.09	7.50 ± 0.02

[a] CQ/Suc, Suc-pretreated cells during cotreatment with CQ and sucrose; CQ/, previously untreated cells; CQ/Baf, cotreatment with CQ and Baf in previously untreated cells.

[b] Values in bold indicate a statistically significant difference from the untreated cells using Tukey's test ($p < 0.05$).

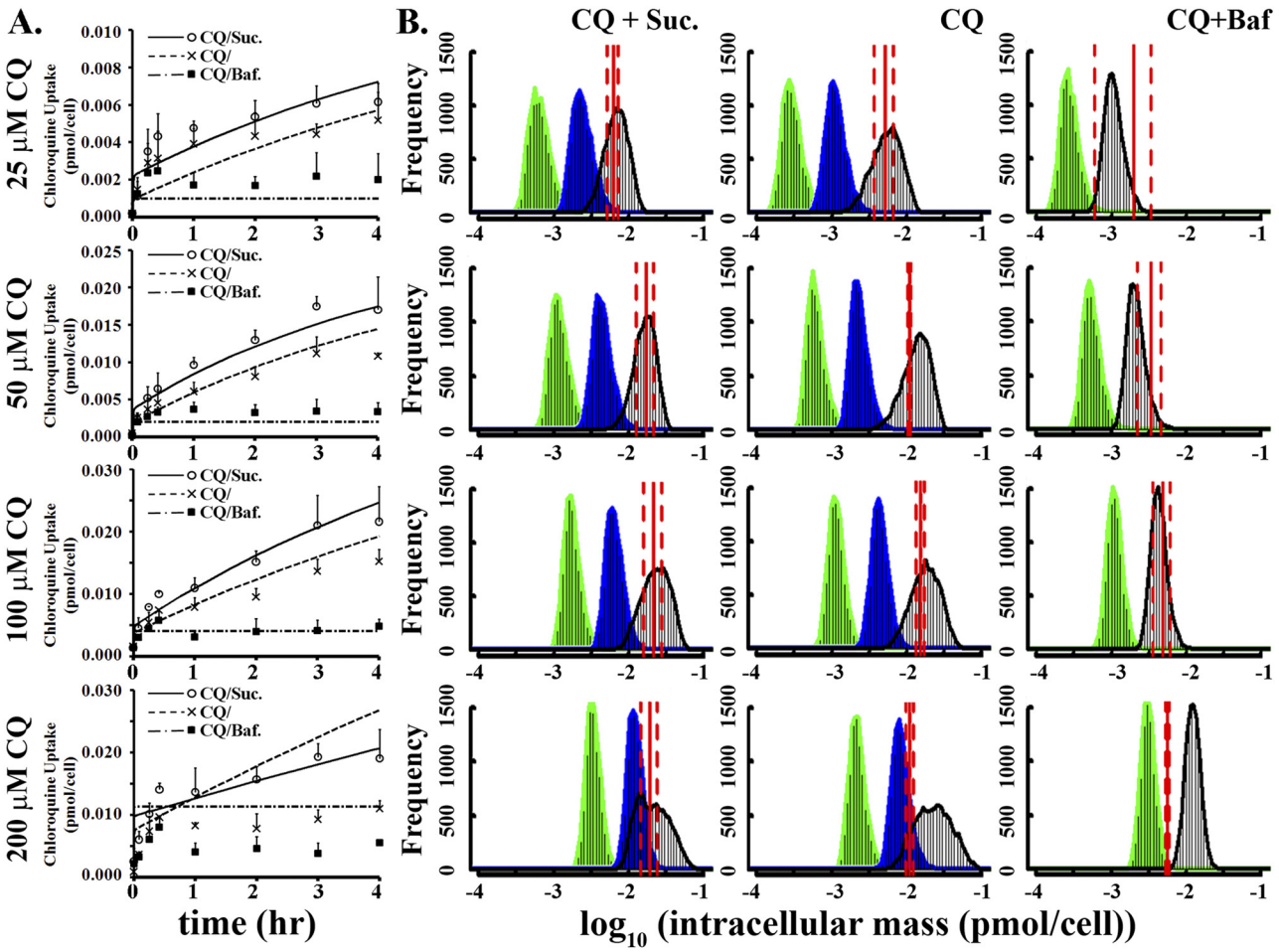

Fig. 5. Quantitative analysis and mechanism-based, predictive pharmacokinetic modeling of CQ uptake in MDCK cells. A, measured uptake kinetics during 1) 25, 50, 100, and 200 μM CQ treatments in previously untreated cells (CQ/); 2) Suc-pretreated cells during cotreatment with CQ and sucrose (CQ/Suc); and 3) cotreatment with CQ and Baf in previously untreated cells (CQ/Baf). Data points correspond to the mean ± S.E.M. (n = 3). B, histograms of Monte Carlo simulations of intracellular CQ accumulation in relation to experimental CQ mass accumulation. A total of 10,000 simulations were performed with parameters randomly selected from a range (Supplemental Table S1). Red solid lines correspond to the measured, average CQ mass per cell at the end of a 4-h incubation with 25, 50, 100, and 200 μM CQ (red dashed lines represent ± S.E.M.). Green indicates simulation results in the absence of phenotypic changes. Blue indicates simulation results incorporating volume changes of organelles but without partitioning to MLB/MVBs. Black indicates simulation results incorporating volume changes in acidic organelles, as well as CQ partitioning to MLBs/MVBs.

For comparison, the simulated intracellular CQ mass at the end of a 4-h incubation period was calculated under three different conditions: 1) in the presence of ion trapping but without expanding organelle volumes nor binding of protonated CQ species to MLBs/MVBs (Fig. 5B, green); 2) in the presence of ion trapping within expanding acidic organelles but without binding of protonated CQ species to MLBs/MVBs (Fig. 5B, blue); and 3) in the presence of ion trapping in expanding acidic organelles, with binding of protonated CQ species to MLBs/MVBs (Fig. 5B, black). Parameter sensitivity analysis (Supplemental Fig. 2) showed that molecular properties including pK_a and logP for the neutral forms or ionized forms; pH and volume in the extracellular compartment; volume in the cytosol; and pH, volume, membrane po-

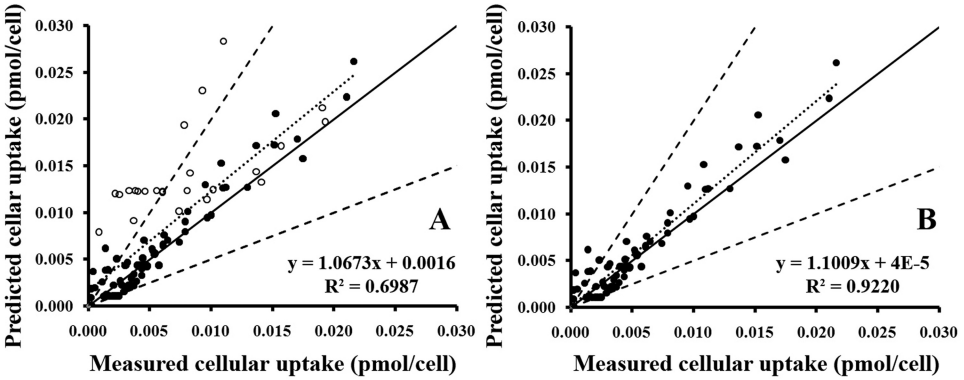

Fig. 6. Assessing the performance of the cellular pharmacokinetic model. The predicted intracellular mass was plotted against the measured values at eight time points for four levels of CQ treatment with (or without) sucrose or bafilomycin A1. ——, the unity line; – – –, factor of 2 on both sides of the unity line; ·····, the best fit with the equation displayed. ●, data from 25, 50, and 100 μM CQ treatments; ○, data from 200 μM CQ treatments. A, analysis of measurements from 25, 50, 100, and 200 μM CQ treatments. B, analysis of measurements from 25, 50, and 100 μM CQ treatments.

tential, ionic strength, and lipid fraction in the lysosomes were important factors (caused a >20% change with parameters randomly sampled from physiologically relevant ranges) for CQ uptake. Then Monte Carlo simulations were performed to calculate a distribution of predicted CQ accumulation values based on a range of these input parameters in cells incubated with CQ alone or in combination with Suc or Baf.

The impact of CQ-induced phenotypic effects on the predicted cellular accumulation of CQ was consistent with most of the intracellular CQ accumulation occurring within the expanding acidic (LTG-positive) vesicles. On the basis of the simulations, the volume increase of acidic organelles led to a >5-fold increase in the predicted intracellular mass (Fig. 5B, green versus blue), whereas adding an MLBs/MVB binding component led to an additional 2-fold increase in intracellular CQ mass (Fig. 5B, blue versus black). Simulation results incorporating vesicular expansion and CQ binding to MLBs/MVBs corresponded to the range of measured values (Fig. 5B, black versus red lines).

The greatest discrepancy between simulation results and experimental measurements was observed in Baf-treated cells. This discrepancy can be ascribed to measurement errors: in Baf, LTG uptake is much reduced and the diameter of acidic vesicles was close to the optical resolution limit of the microscope, so the organelle volume measurements were less precise than for the other conditions. In addition, the accuracy and precision of CQ mass measurement in the presence of Baf was considerably lower than that in the other experimental conditions, because the CQ signal in Baf was almost undetectable.

Discussion

In this study, we used MDCK cells exposed to 0 to 200 μM CQ as a physiologically relevant in vitro experimental model to analyze CQ pharmacokinetics in cells of the distal renal tubule. We present quantitative evidence that the phospholipidosis-like phenotypic effect induced by CQ may be responsible for the observed, nonsteady-state intracellular accumulation of CQ. In the process, we elaborated a computational in silico model for simulating how phospholipidosis affects the cellular pharmacokinetics of small-molecule drugs. As a physiologically relevant transport probe, CQ is a weak base drug for treatments of malaria, arthritis, viral infection, and cancer (Djordevic et al., 1992; Pardridge et al., 1998). Despite its high solubility, CQ has slow clearance, accumulates in kidney (and other organs) >1000-fold relative to plasma concentrations, and has highly variable pharmacokinetics with the elimination half-life ranging from 20 to 60 days (Ducharme and Farinotti, 1996). Significant variability in CQ pharmacokinetics have been ascribed to differences in protein binding, but functional differences in renal filtration could also be involved because the drug is mostly cleared by the kidney (Krishna and White, 1996).

Previous studies established that CQ reached high concentrations inside cells with particularly high levels in the lysosomes (Hostetler et al., 1985), presumably by the action of a carrier-mediated active transport mechanism. However, although CQ may be a substrate of multiple drug resistance 1 protein (Polli et al., 2001) and organic cation transporter-like 2 protein (Reece et al., 1998), both of these are involved in the excretion of drugs from cytosol to the extracellular medium. No active transporter mechanisms have been found to play a role in CQ cellular uptake. OCT2 plays important roles in the uptake of cationic compounds in the kidney, but chloroquine does not appear to interact with OCT2 (Zolk et al., 2009). In fact, unlike uptake of other organic cations that are substrates of an active transporter [i.e., plasma membrane monoamine transporter (PMAT)] (Engel and Wang, 2005), the cellular uptake of CQ did not depend on the sodium concentration in the extracellular medium (Fig. 4, B and C). In addition, although low pH in the extracellular medium has been found to stimulate the uptake of PMAT substrates, we found it significantly inhibited CQ uptake. Last, PMAT and OCTs are not extensively expressed in normal, distal tubular cells (Karbach et al., 2000; Xia et al., 2009). Therefore, all available evidence indicates that CQ crosses biological membranes of MDCK cells by passive diffusion (Fig. 4A). We found that many pharmacological OCTs inhibitors did not affect cellular uptake of CQ (Fig. 4, A–C), whereas all treatments that directly affected the cellular vacuolation response did affect CQ uptake.

Microscopically, the appearance of MLBs/MVBs in MDCK cells treated with CQ corresponded to the morphology of kidney cells of CQ-treated patients, as well as that of other cells after exposure to weakly basic, lipophilic drugs (Hallberg et al., 1990; Müller-Höcker et al., 2003; Marceau et al., 2009). The size of the expanded vesicles and the internal vesicles as measured by fluorescence microscopy and transmission electron microscopy were comparable (Figs. 1 and 2). The discrepancy between the absolute values of these two measurements can be ascribed to differences in sample preparation as well as the resolution of these two instruments. With fluorescence microscopy, the samples are fresh and immersed in a living cell environment, whereas with EM the samples are dehydrated. Second, for TEM sample preparation, cells are sliced with a ultramicrotome so the diameter of the vesicles in TEM images might not be the actual equatorial diameter. As a result, the measured sizes of the expanded vesicles in TEM images were smaller than measurements from fluorescent images. When the measured sizes of internal vesicles in MLBs/MVBs are compared, the discrepancy in measured sizes was not significant, considering the relatively low resolution of the fluorescence microscopy (1 pixel = 0.047 μm in this study).

Meanwhile, a close relationship between CQ-induced volume expansion of LTG-positive vesicles and CQ uptake was observed (Fig. 4, B and C). Accordingly, we measured the cellular pharmacokinetics of CQ in dose-response and time course experiments. In turn, these measurements were compared with simulation results obtained by modeling intracellular CQ mass accumulation under three different scenarios: 1) in the absence of CQ-induced phenotypic effects; 2) in the presence of expanding acidic organelles; and 3) in the presence of expanding acidic organelles coupled to binding to intraluminal MLBs/MVBs. We found that the latter condition yielded results that were consistent with the measured absolute CQ levels as well as the relative changes of intracellular CQ mass under different experimental conditions.

Supporting a role for MLBs/MVBs in the sequestration of CQ, LTG (a weakly basic fluorescent probe that accumulates in acidic organelles due to ion trapping) was visibly concentrated within MLBs/MVBs in the lumen of expanded cytoplasmic vesicles induced by CQ. The inability of 3MA to inhibit the phenotypic effects induced by CQ suggests that

the phospholipidosis effects of CQ are not due to an induced, autophagocytic mechanism. Experiments and simulations of CQ uptake in combination with Suc provided evidence that stimulating the phospholipidosis-like phenotype facilitates CQ accumulation. Experiments and simulations of CQ uptake in combination with Baf provided evidence that inhibiting the phospholipidosis-like phenotype decreases CQ accumulation. Last, Raman confocal microscopy confirmed that intracellular CQ accumulates within the expanded, CQ-induced cytoplasmic vesicles with intraluminal MLBs/MVBs, as predicted by the model. Phospholipids such as phosphatidylcholine have very high affinity for protonated CQ (Kuroda and Saito, 2010), consistent with most of the protonated CQ within the expanded vesicles being bound to the membranes of intraluminal MLBs/MVBs.

It is also noteworthy that intracellular transformation of CQ into a less membrane-permeant CQ metabolite cannot account for its continuous accumulation in MDCK cells. Previously we demonstrated that intracellular CQ in MDCK cells is mostly present in intact form (Zhang et al., 2010). Although passive diffusion coupled to ion trapping and phospholipid binding can explain the observed transport behaviors, we also searched for an active transport mechanism driving CQ accumulation. However, the effects of bafilomycin and sucrose, the lack of effect of active transport inhibitors, the correlation between vacuolar expansion and the accumulation of CQ, the pH sensitivity of CQ uptake, the insensitivity to extracellular sodium, and the linear concentration dependence of CQ uptake all made it very difficult to relate the behavior of CQ to candidate active transport mechanisms.

To conclude, our results provide evidence that the phospholipidosis effects of CQ may underlie an inducible, highly effective, intracellular weak base sequestration system. To our knowledge, this is the first study to evaluate the potential effects of phospholipidosis on the cellular pharmacokinetic behavior of a weakly basic molecule. Our simulations and experimental results converged on changes in organelle structure and membrane organization induced by CQ that could profoundly alter the intracellular bioaccumulation and distribution of CQ according to its passive transport properties, leading to the nonsteady-state accumulation behavior. Considering that similar morphological changes are induced by other weak base drugs that accumulate intracellularly, such as procainamide and amiodarone (Morissette et al., 2009), the phospholipidosis phenotype warrants consideration as candidate, mechanistic determinant of the local (and systemic) distribution and disposition of weakly basic lipophilic molecules in the tissues and organs of the body, especially in cells exposed to high local concentrations of the drug. Passive transport models have been successfully used for developing predictive physiologically based pharmacokinetic models of bioaccumulation and biodistribution of neutral or ionized organic compounds in tissues and organs (Fu et al., 2009; Trapp et al., 2010; Yu and Rosania, 2010). For weakly basic molecules, incorporation of the cellular pharmacokinetic effects of phospholipidosis may considerably improve physiologically based pharmacokinetic and biodistribution predictions.

Acknowledgments

We thank Dorothy Sorenson at the Microscopy and Image-analysis Laboratory for assistance with TEM work. We also thank Dr. Adam Matzger at the Department of Chemistry, University of Michigan, for help with Raman confocal microscopy.

Authorship Contributions

Participated in research design: Zheng and Rosania.
Conducted experiments: Zheng and Zhang.
Performed data analysis: Zheng.
Wrote or contributed to the writing of the manuscript: Zheng, Zhang, and Rosania.
Other: Rosania acquired funding for the research.

References

Bawolak MT, Morissette G, and Marceau F (2010) Vacuolar ATPase-mediated sequestration of local anesthetics in swollen macroautophagosomes. *Can J Anaesth* **57:**230–239.
Bergqvist Y, Hed C, Funding L, and Suther A (1985) Determination of chloroquine and its metabolites in urine: a field method based on ion-pair extraction. *Bull World Health Organ* **63:**893–898.
de Duve C, de Barsy T, Poole B, Trouet A, Tulkens P, and Van Hoof F (1974) Commentary. Lysosomotropic agents. *Biochem Pharmacol* **23:**2495–2531.
Djordevic B, Lange CS, and Rotman M (1992) Potentiation of radiation lethality in mouse melanoma cells by mild hyperthermia and chloroquine. *Melanoma Res* **2:**321–326.
Ducharme J and Farinotti R (1996) Clinical pharmacokinetics and metabolism of chloroquine. Focus on recent advancements. *Clin Pharmacokinet* **31:**257–274.
Duvvuri M and Krise JP (2005) A novel assay reveals that weakly basic model compounds concentrate in lysosomes to an extent greater than pH-partitioning theory would predict. *Mol Pharm* **2:**440–448.
Engel K and Wang J (2005) Interaction of organic cations with a newly identified plasma membrane monoamine transporter. *Mol Pharmacol* **68:**1397–1407.
Fu W, Franco A, and Trapp S (2009) Methods for estimating the bioconcentration factor of ionizable organic chemicals. *Environ Toxicol Chem* **28:**1372–1379.
Gong Y, Zhao Z, McConn DJ, Beaudet B, Tallman M, Speake JD, Ignar DM, and Krise JP (2007) Lysosomes contribute to anomalous pharmacokinetic behavior of melanocortin-4 receptor agonists. *Pharm Res* **24:**1138–1144.
Gruenberg J and Stenmark H (2004) The biogenesis of multivesicular endosomes. *Nat Rev Mol Cell Biol* **5:**317–323.
Hallberg A, Naeser P, and Andersson A (1990) Effects of long-term chloroquine exposure on the phospholipid metabolism in retina and pigment epithelium of the mouse. *Acta Ophthalmol (Copenh)* **68:**125–130.
Hayeshi R, Masimirembwa C, Mukanganyama S, and Ungell AL (2008) Lysosomal trapping of amodiaquine: impact on transport across intestinal epithelia models. *Biopharm Drug Dispos* **29:**324–334.
Helip-Wooley A and Thoene JG (2004) Sucrose-induced vacuolation results in increased expression of cholesterol biosynthesis and lysosomal genes. *Exp Cell Res* **292:**89–100.
Heuser J (1989) Changes in lysosome shape and distribution correlated with changes in cytoplasmic pH. *J Cell Biol* **108:**855–864.
Honegger UE, Quack G, and Wiesmann UN (1993) Evidence for lysosomotropism of memantine in cultured human cells: cellular kinetics and effects of memantine on phospholipid content and composition, membrane fluidity and β-adrenergic transmission. *Pharmacol Toxicol* **73:**202–208.
Hostetler KY, Reasor M, and Yazaki PJ (1985) Chloroquine-induced phospholipid fatty liver. Measurement of drug and lipid concentrations in rat liver lysosomes. *J Biol Chem* **260:**215–219.
Hostetler KY and Richman DD (1982) Studies on the mechanism of phospholipid storage induced by amantadine and chloroquine in Madin Darby canine kidney cells. *Biochem Pharmacol* **31:**3795–3799.
Karbach U, Kricke J, Meyer-Wentrup F, Gorboulev V, Volk C, Loffing-Cueni D, Kaissling B, Bachmann S, and Koepsell H (2000) Localization of organic cation transporters OCT1 and OCT2 in rat kidney. *Am J Physiol Renal Physiol* **279:**F679–F687.
Krishna S and White NJ (1996) Pharmacokinetics of quinine, chloroquine and amodiaquine. Clinical implications. *Clin Pharmacokinet* **30:**263–299.
Kuroda Y and Saito M (2010) Prediction of phospholipidosis-inducing potential of drugs by in vitro biochemical and physicochemical assays followed by multivariate analysis. *Toxicol In Vitro* **24:**661–668.
Marceau F, Bawolak MT, Bouthillier J, and Morissette G (2009) Vacuolar ATPase-mediated cellular concentration and retention of quinacrine: a model for the distribution of lipophilic cationic drugs to autophagic vacuoles. *Drug Metab Dispos* **37:**2271–2274.
Morissette G, Ammoury A, Rusu D, Marguery MC, Lodge R, Poubelle PE, and Marceau F (2009) Intracellular sequestration of amiodarone: role of vacuolar ATPase and macroautophagic transition of the resulting vacuolar cytopathology. *Br J Pharmacol* **157:**1531–1540.
Müller-Höcker J, Schmid H, Weiss M, Dendorfer U, and Braun GS (2003) Chloroquine-induced phospholipidosis of the kidney mimicking Fabry's disease: case report and review of the literature. *Hum Pathol* **34:**285–289.
Nilsson C, Kågedal K, Johansson U, and Ollinger K (2003) Analysis of cytosolic and lysosomal pH in apoptotic cells by flow cytometry. *Methods Cell Sci* **25:**185–194.
Pardridge WM, Yang J, and Diagne A (1998) Chloroquine inhibits HIV-1 replication in human peripheral blood lymphocytes. *Immunol Lett* **64:**45–47.
Piper RC and Katzmann DJ (2007) Biogenesis and function of multivesicular bodies. *Annu Rev Cell Dev Biol* **23:**519–547.
Polli JW, Wring SA, Humphreys JE, Huang L, Morgan JB, Webster LO, and

Serabjit-Singh CS (2001) Rational use of in vitro P-glycoprotein assays in drug discovery. *J Pharmacol Exp Ther* **299:**620–628.
Reasor MJ and Kacew S (2001) Drug-induced phospholipidosis: are there functional consequences? *Exp Biol Med (Maywood)* **226:**825–830.
Reece M, Prawitt D, Landers J, Kast C, Gros P, Housman D, Zabel BU, and Pelletier J (1998) Functional characterization of ORCTL2—an organic cation transporter expressed in the renal proximal tubules. *FEBS Lett* **433:**245–250.
Rindler MJ, Chuman LM, Shaffer L, and Saier MH Jr (1979) Retention of differentiated properties in an established dog kidney epithelial cell line (MDCK). *J Cell Biol* **81:**635–648.
Saftig P and Klumperman J (2009) Lysosome biogenesis and lysosomal membrane proteins: trafficking meets function. *Nat Rev Mol Cell Biol* **10:**623–635.
Trapp S, Franco A, and Mackay D (2010) Activity-based concept for transport and partitioning of ionizing organics. *Environ Sci Technol* **44:**6123–6129.
Trapp S and Horobin RW (2005) A predictive model for the selective accumulation of chemicals in tumor cells. *Eur Biophys J* **34:**959–966.
Walker O, Dawodu AH, Adeyokunnu AA, Salako LA, and Alvan G (1983) Plasma chloroquine and desethylchloroquine concentrations in children during and after chloroquine treatment for malaria. *Br J Clin Pharmacol* **16:**701–705.
Wilson PD, Firestone RA, and Lenard J (1987) The role of lysosomal enzymes in killing of mammalian cells by the lysosomotropic detergent *N*-dodecylimidazole. *J Cell Biol* **104:**1223–1229.
Xia L, Zhou M, Kalhorn TF, Ho HT, and Wang J (2009) Podocyte-specific expression of organic cation transporter PMAT: implication in puromycin aminonucleoside nephrotoxicity. *Am J Physiol Renal Physiol* **296:**F1307–F1313.
Yu JY and Rosania GR (2010) Cell-based multiscale computational modeling of small molecule absorption and retention in the lungs. *Pharm Res* **27:**457–467.
Zhang X, Shedden K, and Rosania GR (2006) A cell-based molecular transport simulator for pharmacokinetic prediction and cheminformatic exploration. *Mol Pharm* **3:**704–716.
Zhang X, Zheng N, Zou P, Zhu H, Hinestroza JP, and Rosania GR (2010) Cells on pores: a simulation-driven analysis of transcellular small molecule transport. *Mol Pharm* **7:**456–467.
Zolk O, Solbach TF, König J, and Fromm MF (2009) Structural determinants of inhibitor interaction with the human organic cation transporter OCT2 (SLC22A2). *Naunyn Schmiedebergs Arch Pharmacol* **379:**337–348.

Address correspondence to: Dr. Gus R. Rosania, Department of Pharmaceutical Sciences, University of Michigan College of Pharmacy, 428 Church St., Ann Arbor, MI 48109. E-mail: grosania@umich.edu